Edinburgh Research Explorer

Phytochromes control metabolic flux, and their action at the seedling stage determines adult plant biomass

1 **Article title:** Phytochromes control metabolic flux, and their action at the seedling

2 stage determines adult plant biomass

3 **Running title:** Metabolic flux and growth in phytochrome mutants

4 **Authors:** Johanna Krahmer[1,4], Ammad Abbas[1], Virginie Mengin[2], Hirofumi

5 Ishihara[2], Andrés Romanowski[1], James J. Furniss[1,5], Thiago Alexandre Moraes[2],

6 Nicole Krohn[2], Maria Grazia Annunziata[2], Regina Feil[2], Saleh Alseekh[2], Toshihiro

7 Obata[2,3], Alisdair R Fernie[2], Mark Stitt[2], Karen J. Halliday[1]

8

9 **Author addresses:**

10 [1]Institute for Molecular Plant Science, School of Biological Sciences, Daniel

11 Rutherford Building, Building, Max Born Crescent, Kings Buildings, University of

12 Edinburgh, Edinburgh, EH9 3BF, United Kingdom

13 [2]Max Planck Institute of Molecular Plant Physiology, Potsdam - Golm 14476,

14 Germany

15 [3]Institute of Agriculture and Natural Resources, Department of Biochemistry,

16 University of Nebraska, Lincoln, Nebraska, USA

17 [4]Center for Integrative Genomics, Faculty of Biology and Medicine, University of

18 Lausanne, 1015 Lausanne, Switzerland

19 [5]Division of Genetics and Genomics, Roslin Institute, University of Edinburgh, Easter

20 Bush, Edinburgh EH25 9RG, United Kingdom

21

22 **Author email addresses**:

23 JK, johanna.krahmer@unil.ch; AA, Ammad.Abbas@ed.ac.uk; VM,

24 Mengin@mpimp-golm.mpg.de; HI, Ishihara@mpimp-golm.mpg.de; AR,

25 Andrew.Romanowski@ed.ac.uk; JF, James.Furniss@ed.ac.uk; TAM,

26 Moraes@mpimp-golm.mpg.de; NK, Krohn@mpimp-golm.mpg.de; GMA,

27 Annunziata@mpimp-golm.mpg.de; RF, Feil@mpimp-golm.mpg.de; SA,

28 Alseekh@mpimp-golm.mpg.de; TO, tobata2@unl.edu; ARF, Fernie@mpimp-

29 golm.mpg.de; MS, MStitt@mpimp-golm.mpg.de; KJH, karen.halliday@ed.ac.uk

30 **Corresponding Author**: Prof Karen J. Halliday, +44 (0)131 651 9083,

31 karen.halliday@ed.ac.uk

32

33 **date of submission: 27.11.2020**

34 **number of figures:** 4 (all in colour)

35 **word count:** 6422

36 **number of supplementary figures:** 11

37 **number of supplementary tables:** 1

38 **number of supplementary datasets**: 1

39

40 **Highlight**: Phytochrome photoreceptors affect the synthesis rates of primary

41 metabolites and their action at the seedling stage is a key determinant of adult plant

42 biomass.

43

44 **Abstract**

45 Phytochrome (phy) photoreceptors are known to regulate plastic growth responses to

46 vegetation shade. However, recent reports also suggest an important role for phys in

47 carbon resource management, metabolism, and growth. Here, we use $^{13}CO_2$ labelling

48 patterns in multi-allele *phy* mutants to investigate the role of phy in the control of

49 metabolic fluxes. We also combine quantitative data of ^{13}C incorporation into protein

50 and cell wall polymers, gas exchange measurements and system modelling to

51 investigate why biomass is decreased in adult multi-allele *phy* mutants. Phy

52 influences the synthesis of stress metabolites like raffinose and proline, and the

53 accumulation of sugars, possibly through regulating vacuolar sugar transport.

54 Remarkably, despite their modified metabolism and vastly altered architecture,

55 growth rates in adult *phy* mutants resemble those of wild-type plants. Our results

56 point to delayed seedling growth and smaller cotyledon size as the cause of the adult-

57 stage *phy* mutant biomass defect. Our data signify a role for phy in metabolic stress

58 physiology, carbon partitioning and illustrate that phy action at the seedling stage sets

59 the trajectory for adult biomass production.

60

61 **Keywords**: ^{13}C labelling, growth modelling, metabolic flux, phytochrome, plant

62 growth, stress metabolites

63

64 **Abbreviations**: DAS – days after sowing; EoD – end of day; FR – far-red light; phy

65 – phytochrome; R – red light; RGR – relative growth rate; SAR – shade avoidance

66 response; WT – wildtype; ZT – zeitgeber time

67

68

69

<u>Introduction</u>

70 Phytochrome (phy) light receptors are major regulators of growth plasticity, a
71 fundamental characteristic that ensures plants adapt to a changing environment. The
72 shade avoidance response (SAR) is a common adaptive growth strategy in vegetation-
73 rich habitats, where competition for light and other resources can be intense. In
74 Arabidopsis, a rosette plant, SAR features include increased petiole elongation and
75 reduced leaf blade area. These large changes in leaf architecture require modifications
76 of leaf development and carbon resource management (Yang *et al*, 2016). While we
77 have a good appreciation of the molecular events that underlie the SAR, our
78 knowledge of the concomitant metabolic changes is more rudimentary.

79

80 In nature, the light that a plant experiences through a day is strongly affected by its
81 immediate environment. Through shading, the vegetation canopy can restrict access
82 to light and can alter spectral quality, increasing the proportion of far-red (FR)
83 compared to red (R) wavelengths. Phy photochemistry is tuned to detect these
84 vegetation-induced changes in light quality and quantity. The phys exist as two
85 reversible isomeric forms Pr and Pfr. R light induces Pr photoconversion to the active
86 Pfr form, while FR switches Pfr back to inactive Pr. Changes in the R:FR ratio within
87 vegetation-rich habitats drive the dynamic equilibrium of Pr:Pfr, and the proportion of
88 active Pfr (Rausenberger *et al*, 2010). Light independent relaxation of Pfr to inactive
89 Pr, can also occur through a process known as dark or thermal reversion, enabling
90 sensitive detection of fluence rate and temperature (Rausenberger *et al*, 2010; Casal,
91 2013). Thus, vegetation canopy conditions reduce the pool of active Pfr, which in
92 turn, activates the adaptive SAR growth strategy.

93

94 In seedlings, SAR is typified by elongation of hypocotyls, delayed apical hook
95 opening, reduced cotyledon size, and low chlorophyll content (Franklin and Whitelam
96 2005; Leivar et al. 2008; Chen and Chory 2011; Hu et al. 2013). In adult plants, SAR
97 features include elongated petioles, smaller leaf blades, increased leaf hyponasty,
98 reduced leaf emergence rate and early flowering (Halliday *et al*, 2003; Casal, 2013).
99 In Arabidopsis, there are five phys designated phyA-phyE. The contribution of
100 different phys to the regulation of SAR can be assessed by investigating the extent to
101 which mutations in different phytochromes lead to a SAR phenotype in non-shade

3

light. While phyB is known to have a central role in SAR, the other phys also have important contributory roles, evident in allelic series (e.g *phyB*, *phyBD*, *phyABD* and *phyABDE)*, which display incremental increases in the severity of the SAR phenotype (Hu *et al*, 2013; Yang *et al*, 2016).

We have a growing understanding of the molecular pathways that underlie SAR. Members of PHYTOCHROME INTERACTING FACTOR (PIF1, 3, 4, 5, 7) clade of bHLH transcription factors are pivotal actors in the promotion of SAR. Active phyB Pfr binds directly to PIFs to suppress their activity, either by reducing their DNA-binding capacity (shown for PIF1, PIF3 and PIF4) or by promoting PIF phosphorylation, ubiquitination and degradation by the 26S proteasome (Leivar *et al*, 2012; Legris *et al*, 2019). Canopy shade conditions that diminish phyB Pfr, lead to increased abundance and activity of PIFs, which alters the expression of a range of different targets, notably auxin synthesis and signalling genes that play a central role in SAR.

The changed growth pattern during SAR is presumably underpinned by changes in metabolism. These might plausibly include changes in the allocation of resources between storage, growth, i.e., the synthesis of cellular components like protein and cell wall polymers, and stress responses. Indeed, it is increasingly clear from work in seedlings that phytochrome controls critical aspects of carbon metabolism. In *Arabidopsis* seedlings, phytochrome is required for mobilisation of seed oil reserves during de-etiolation (Kozuka *et al*, 2020). phyB and PIF1, PIF3, PIF4 and PIF5 have been shown to have regulatory functions in sucrose promotion of hypocotyl elongation (Stewart *et al*, 2011; Lilley-Steward *et al*, 2012). Phys are proposed to be involved in promoting seedling root growth by cotyledon-derived sucrose (Kircher & Schopfer, 2012). Work in *Brassica* seedlings illustrates that the proportion of assimilated carbon that is partitioned to the hypocotyl doubles in response to low R:FR conditions (de Wit *et al*, 2018). Complementary analysis of Arabidopsis seedlings suggests this response is mainly dependent on PIF7, with contributions from PIF4 and / or PIF5 (de Wit *et al*, 2018). Thus, in seedlings phys are not only required for altered molecular signalling but also reprogramming of carbon resource management.

136

137 Much less is known about the impact of phy signalling on the metabolism and growth
138 of adult plants. Our published work using GC-MS has shown that SAR-induced
139 architectural changes in adult plants are accompanied by marked changes in
140 metabolite levels and partitioning, including higher rosette sugar content (Yang *et al*,
141 2016). We established that in addition to the well-described changes in leaf
142 morphology, phy-deficiency can severely compromise biomass production, for
143 instance, the multi-allele *phyABDE* mutant has an 80% reduction in adult rosette
144 biomass (Yang *et al*, 2016). However, while this initial study described the metabolic
145 and size phenotypes associated with loss of phytochrome function in adult plants, it
146 did not uncover the metabolic basis for these changes. This was partly because only a
147 small number of metabolic intermediates in central metabolism were analysed.
148 Further, on their own, measurements of metabolite levels and plant size do not
149 provide direct information about how and when phytochrome signalling impacts on
150 metabolic fluxes and growth rates.

151

152 In this study, we conducted a dynamic metabolite flux analysis to gain a more in-
153 depth understanding of how phy controls central metabolism. This was accomplished
154 using LC-MS/MS and ^{13}C labelling followed by GC-MS metabolite profiling. Our
155 data show that phy control of carbon-resource management is manifestly different in
156 early and later development. In seedlings, phys can shift the balance between glucose
157 and starch, which is important for hypocotyl elongation. In adult plants, phys control
158 the flux through major metabolic pathways and the *de novo* synthesis of stress
159 metabolites such as proline and raffinose. However, maybe unexpectedly, they have
160 little or no impact on the rate of growth *per se*. Using the multi-scale Framework
161 Model, that integrates environmental and carbon metabolism control of plant growth,
162 we provide a new system-level understanding of why phy-deficiency has such a
163 dramatic impact on adult plant biomass.

164

165 **Materials and Methods**

166

167 **Plant material and growth conditions**

168 We used the model plant species *Arabidopsis thaliana* in all experiments. The *phy*
169 mutants (*phyBD* (Devlin *et al*, 1999), *phyABD* (Devlin *et al*, 1999), *phyABDE*

5

170   (Franklin *et al*, 2003) used in this study were all in the Ler background unless

171   otherwise indicated. All mutants used have been previously described (*phyABD*

172   mutant in Col-0 (Sánchez-Lamas *et al*, 2016), 35S:PIF4-HA and 35S:PIF5-HA

173   (Lorrain *et al*, 2008), *hy5-215* (Oyama *et al*, 1997).

174

175   Seeds were surface sterilised with 30% thin bleach and 0.01% TritonX-100, washed 5

176   times with sterile water and stratified at 4°C for 4 to 5 days in ddH$_2$O. For gas

177   exchange measurements and the 5-week growth curve analysis, where plants were

178   grown entirely on soil, and 200µM GA4+7 (Duchefa) was added to the water during

179   stratification and washed off before placing on soil to improve germination of the

180   higher-order *phy* mutants (Sánchez-Lamas *et al*, 2016).

181

182   With the exception of gas exchange experiments and the growth curves, stratified

183   seeds were placed on plates (1/2 MS pH5.8, 1.2% agar), and grown at 18°C and

184   115µmol m^{-2} s^{-1} either in LD8:16 photoperiods for experiments with 5-week old

185   plants or in LD12:12 photoperiods for experiments with younger plants. Seedlings

186   were transferred to soil at 14 (for experiments with 5-week old plants) or 10 DAS

187   (most experiments with younger plants) or 7 DAS (labelling experiments 2 and 3).

188   Growth conditions were kept the same after transfer to soil except for experiments on

189   5-week old plants where the light regime was switched to LD12:12 at 14 DAS.

190

191   These conditions (18°C, 115µmol m^{-2} s^{-1} and LD12:12 or LD8:16 followed by

192   LD12:12) were used for all experiments unless otherwise stated. Exceptions were for

193   the experiments testing the conditionality of metabolite over-accumulation

194   (Supplementary Fig. S6, see next section), and the growth curve experiment was

195   carried out in LD12:12 entirely. For metabolite measurement in seedlings, seeds were

196   directly sown on soil. The same-biomass wildtype (WT) control in labelling

197   experiment 1 and the LC-MS experiment was also grown at LD8:16 for 2 weeks and

198   then at LD12:12 until harvesting at 30 DAS.

199

200   In Supplementary Fig. S6 we tested the robustness of metabolite profiles to

201   deviations from our reference conditions described above. For measurement in

202   different photoperiods (Supplementary Fig. S6A-C), plants were either kept at

203   LD8:16 after the initial 2 weeks in short days, or moved to either LD12:12 or

204   LD16:8 for the remaining 3 weeks. To test the effect of light intensity

205   (Supplementary Fig. S6D-F), plants were grown in our reference conditions but

206   were moved to different light intensities for the last 3 days before sampling at

207   the end of the day. For temperature experiments (Supplementary Fig. S6G-I),

208   plants were moved to either 16°C or 22°C 4 days prior to sampling.

209

210   In labelling experiments 2 and 3, plating and transfer of WT, *phyABD* and *phyABDE*

211   had to be staggered by 1 day as transfer took too long to complete all three genotypes

212   in one day. This allowed labelling and sampling on the same working day in identical

213   labelling conditions at ages 17, 18 and 19 DAS. Experiments 2 and 3 were identical

214   except that different seed batches were used.

215

216   EoD sampling was done within the last 30min of the light period. Samples were taken

217   in three replicates with at least 5 plants per replicate. Tissue was quickly cut and

218   flash-frozen in liquid nitrogen. In the case of plants for LC-MS analysis of

219   phosphorylated and short half-life metabolites (Fig. 1), rosettes were flash-frozen in a

220   mortar inside the incubator without changing the light exposure of the cut rosette

221   before freezing (Arrivault *et al*, 2009; Szecowka *et al*, 2013).

222   Without allowing the tissue to thaw, samples were ground with metal balls using a

223   Qiagen TissueLyzer and aliquots were weighed out. Aliquot weights were recorded

224   for normalisation.

225

226   **^{13}C labelling**

227   ^{13}C labelling with air containing only $^{13}CO_2$ was carried out as described (Ishihara *et*

228   *al*, 2015), was started at light onset and continued for 24h. Samples were taken in

229   triplicates, with 5 plants per replicate for experiment 1, 25 to 30 plants for

230   experiments 2 and 3, at ZT0 (unlabelled), ZT2, ZT12 and ZT24.

231

232   **Metabolite measurements by enzymatic assay**

233   All soluble metabolites (glucose, fructose, malate, fumarate, proline) were measured

234   from ethanolic extracts of about 20mg ground tissue as described (Cross *et al*, 2006;

235   Woodrow *et al*, 2017). Glucose units from starch were measured from hydrolysate of

236   the ethanol insoluble pellet after ethanolic extraction (Cross *et al*, 2006). Protein

237   content for Fig. 3A and Supplementary Fig. S8A was carried out by standard

238   Bradford assay.

239

240   **Gene expression analysis by qRT-PCR**

241   For qRT-PCR analysis, three week old plants were used. Total RNA was isolated

242   from approx. 70mg of finely ground tissue using Qiagen's RNeasy Plant Mini Kit

243   with on-column RNAase-free DNase digestion. cDNA synthesis was performed using

244   the qScript cDNA Supermix (Quanta Biosciences) as described by the manufacturer.

245   The qRT-PCR was set up as a 10µL reaction using SYBR Green (Roche) in a 384-

246   well plate, performed with a Lightcycler-480 system (Roche). Results were analysed

247   using the Light Cycler-480 software. Expression values of target genes were

248   normalized to the *PP2AA3* reference gene and qPCR was repeated for selected time

249   points with *UBQ4* (AT5G20620) as an alternative reference gene (primers see

250   Supplementary Table S1 at *JXB* online).

251

252   **Gene expression by RNA-seq**

253   *RNA extraction and cDNA library preparation and high throughput sequencing*

254   Whole plants were harvested in RNA*later*™ (ThermoFisher Scientific). Once all

255   samples were collected, leaf 3 primordias and leaf 3 blades were dissected with a

256   scalpel, in a Petri dish filled with RNA later solution, under a Leica MZ 16 F

257   dissecting microscope. Total RNA was extracted using the RNeasy Plant Mini Kit

258   (Qiagen) with on-column DNase digestion. Samples were then sent to Edinburgh

259   Genomics for QC check and sequencing. Briefly, quality check of the samples was

260   performed using Qubit with the broad range RNA kit (Thermo Fisher Scientific)

261   and Tapestation 4200 with the RNA Screentape for eukaryotic RNA analysis

262   (Agilent). Libraries were prepared using the TruSeq Stranded mRNA kit

263   (Illumina), and then validated. Samples were pooled to create 14 multiplexed

264   DNA libraries, which were paired-end sequenced on an Illumina HiSeq 4000

265   platform.

266

267   *Read mapping and differential gene expression analysis*

268 Sequence reads were aligned against the Arabidopsis thaliana genome (TAIR10)
269 with TopHat v2.1.1 (Kim *et al*, 2013) with default parameters, except in the case
270 of the maximum intron length parameter, which was set at 5000. Count tables
271 for the different feature levels were obtained from bam files using the ASpli
272 package version 1.6.0 (Mancini *et al*, 2019) with custom R scripts and
273 considering the AtRTD2 transcriptome (Zhang *et al*, 2017).
274 Differential gene expression analysis was conducted for 18,934 genes whose
275 expression was above a minimum threshold level (read density > 0.05) in at least
276 one experimental condition. Read density (rd) was computed as the number of
277 reads in each gene divided by its effective length. The term effective length
278 corresponds to the sum of the length of all the exons of a given gene. Differential
279 gene expression was estimated using the edgeR package version 3.22.3
280 (Robinson *et al*, 2009; Lun *et al*, 2016) and resulting p values were adjusted
281 using a false discovery rate (FDR) criterion. Genes with FDR values lower than
282 0.1 and a log2 fold change > 0.58 were considered to be differentially expressed.
283 Plots were generated using R.
284

285 **Sample preparation for LC-MS/MS analysis**
286 For LC-MS analysis of metabolite abundance at ZT6 and ZT24, metabolites were
287 extracted from ~15mg tissue aliquots. Measurements and data analysis were carried
288 out as in Lunn *et al*, 2006) and modifications described previously (Lunn *et al*, 2006;
289 Arrivault *et al*, 2009; Figueroa *et al*, 2016).
290

291 **Sample preparation for GC-MS analysis**
292 Soluble metabolites were extracted from ~30mg aliquots with methanol, followed by
293 phase separation with chloroform and water (Arrivault *et al*, 2009; Ishihara *et al*,
294 2015). After drying soluble metabolites or neutralised hydrolysates, samples were
295 derivatised and prepared for GC-MS and mass spectrometrically analysed as in Lisec
296 *et al*, (2006).
297

298 Protein was extracted from the methanol-insoluble pellet. 50μg protein was
299 precipitated with TCA, washed with acetone and subsequently hydrolysed and

300   neutralised. After removal of protein from the sample pellet, starch was degraded, cell

301   wall material was hydrolysed and neutralised (Ishihara *et al*, 2015).

302

303   **Analysis of GC-MS data**

304   The XCalibur[TM] software (Thermo Fisher Scientific Inc., version 2.2 SP1.48, 2011)

305   was used for identification and quantification of metabolite peaks. cdf files were

306   converted to raw files and imported into the Processing Setup tool. Peaks were

307   manually assigned by using standards, retention index and fragmentation spectra from

308   the   metabolite   library   ('110524_modified_TFLIB

309   (Version_20070220_05)_AFE_FEMS-Martin_C13_Sorbitol.xls'   from   the   Golm

310   metabolite database). Peak selection by the XCalibur[TM] Sequence batch processing

311   tool was manually verified or adjusted using the XCalibur[TM] QuanBrowser.

312   The resulting peak abundance data resulted in metabolite abundance as well as ^{13}C

313   enrichment for each metabolite. Intensity was normalised by the ribitol abundance

314   and aliquot FW. The enrichment data was adjusted for natural occurrence of different

315   carbon isotopes using the corrector software version 10 (Huege *et al*, 2014). We

316   estimated label incorporation into individual metabolites by identifying the time point

317   before enrichment saturated, multiplying the enrichment at this time by the

318   abundance, and then normalising the value on that in WT plants. This value is an

319   approximate proxy for the minimum rate of synthesis; it will be an underestimate of

320   the rate of synthesis if enrichment in the precursor is less than 100% and if the

321   metabolite is further metabolised. Relative abundance and relative incorporation of

322   new carbon were reported in Supplementary Fig. S2-5 and ratios of *phy* mutant / WT

323   were computed for heatmaps.

324   Metabolite data from LC-MS/MS and GC-MS can be found in Supplementary Data

325   S1.

326

327   **Relative growth rate (RGR), protein synthesis and degradation rate calculations**

328   RGR (gain in biomass per unit existing biomass per time unit) and protein turnover

329   from labelling data were calculated as described (Ishihara *et al*, 2015). For daytime

330   and overall RGR, ^{13}C incorporation at ZT12 and ZT24 was used, respectively. For

331   night-time RGR, incorporation at ZT12 was subtracted from incorporation at ZT24.

332   For Ks values, incorporation of ^{13}C into alanine in protein hydrolysate was used for

333   the same time points as for RGR. To adjust for differences in free alanine labelling,

334   ^{13}C of free alanine at ZT12 was used for day-time Ks, at ZT24 for overall Ks, and the

335   average of ZT12 and ZT24 for night-time Ks. Degradation rates (Kd) were

336   determined by subtracting RGR from Ks (Ishihara *et al*, 2015).

337   RGR from growth curves was determined as the gain of biomass in one day per

338   existing biomass.

339   For water content measurements (Supplementary Fig. S9A), fresh weight (FW)

340   of groups of seedlings was determined which were then dried at 80°C for 3 days

341   and weighed again for DW and water content was calculated as (FW – DW) / FW

342   * 100%.

343

344   **Photosynthetic gas exchange measurements**

345   For measuring net carbon uptake in 2-week old plants, a multi-chamber system

346   (Kölling *et al*, 2015) together with a LiCOR-7000 CO_2/H_2O was used. Each replicate

347   consisted of a pot with at least 20 plants on soil, and 4 replicates were measured for

348   each genotype. Gas exchange was measured after stabilisation in the chambers for

349   30min. Plants were photographed just before measurement for determination of leaf

350   area and immediately cut off after the measurement to determine total above-ground

351   biomass. Pots with soil were then placed back into the photosynthesis chamber to

352   determine background gas exchange by the soil, which was subtracted from the

353   measurement with plants.

354   For measurement of 4-week old plants the setup described by Mengin *et al*, (2017)

355   was used (LI-6400XT Portable Photosynthesis System with a whole-plant

356   Arabidopsis chamber and 6400-18 RGB light source), with a light intensity of

357   115μmol m^{-2} s^{-1} and 60% humidity and 2 or 3 plants per pot.

358

359   **Simulation of RGR, biomass and rosette area using the *Arabidopsis* framework**

360   **model**

361   Cotyledon area was monitored at EoD from 5 DAS to 10 DAS in WT, *phyABD* and

362   *phyABDE* seedlings growing on soil, 110μmol m^{-2} s^{-1}, 18°C and LD 12:12. Cotyledon

363   area was analysed using Adobe Photoshop. Plants were transplanted to individual pots

364   after imaging and were grown in the same conditions until 27 DAS when their above-

365   ground biomass was measured.

366   The framework model was calibrated by changing the light intensity input to correctly

367   predict the WT 27 DAS biomass from the WT cotyledon area at 7 DAS, which is the

368   day the model predicted emergence under the conditions used. Subsequently, the

369   calibrated model was used to simulate area, RGR and biomass for all three genotypes,

370   setting the parameter 'em' to the measured cotyledon sizes.

371

372

373   **Results**

374

375   **LC-MS/MS analysis reveals phy dependent changes in phosphorylated sugars**

376   **and the sucrose-signalling molecule T6P**

377

378   To gain a more nuanced understanding of how phytochrome influences primary

379   metabolism, we used LC-MS/MS, as it provides a reliable method to quantify

380   phosphorylated intermediates and other central metabolites (Lunn *et al*, 2006;

381   Arrivault *et al*, 2009; Szecowka *et al*, 2013; Figueroa *et al*, 2016). Samples were

382   taken from WT and *phyABD* at 35-days. To control for differences in plant biomass,

383   samples were also taken from 30 day-old WT controls, which have equivalent

384   biomass to 35-day old *phyABD* (Fig. 1A, B, Supplementary Fig. S1). Metabolites

385   were measured during the daytime (ZT6) and at the end of the night (ZT24).

386

387   Compared to WT plants, *phyABD* contained elevated levels of many TCA

388   intermediates like succinate, iso-citrate and malate, concurring with (Yang *et al*,

389   2016). Fumarate resembled malate apart from ZT6 in the LC-MS/MS experiment

390   when levels were lower in *phyABD* (Fig. 1A, B, Supplementary Fig. S1). As typically

391   seen in Arabidopsis, malate and fumarate are present at much higher levels than other

392   TCA intermediates. In the WT they accumulate in the daytime and decline at night

393   (Fig 1B, Supplementary Fig. S1). The decline during the night was less marked in

394   *phyABD*. The glycolysis intermediates phospho*enol*pyruvate (PEP) and 3-

395   phosphoglycerate (3-PGA) were lower in *phyABD* than in WT plants, especially

396   during the daytime (Fig 1B, Supplementary Fig. S1). Together with the generally

397   elevated levels of organic acids, this points to a shift of metabolism towards organic

398   acid accumulation.

399

400 The *phyABD* mutant has higher daytime levels of phosphorylated sugars like glucose-
401 1-phosphate (Glc1P) and UDP glucose (UDPG), which are precursors for sucrose,
402 starch and cell wall synthesis. Galactose 1-phosphate (Gal1P), which is the precursor
403 of galactose, has slightly raised levels in *phyABD* (Fig. 1, Supplementary Fig. S1). On
404 the other hand, sucrose-6-phosphate (Suc6P; a dedicated intermediate in sucrose
405 synthesis) and ADP-glucose (ADPGlc; a dedicated intermediate in starch synthesis)
406 were similar in *phyABD* and WT plants. During the daytime, *phyABD* had >50%
407 higher levels of trehalose-6-phosphate T6P (Fig. 1, Supplementary Fig. S1), which
408 has signalling functions that relay information about carbohydrate availability
409 (Yadav *et al*, 2014; Lunn *et al*, 2014; Figueroa *et al*, 2016),

410

411 Overall, these data indicate that phy depletion leads to a shift in the balance between
412 synthesis and breakdown of TCA components and phosphorylated sugars that act as
413 precursors for many metabolic pathways, and modifies the level of carbon-signalling
414 metabolite T6P. It is known that elevated T6P stimulates post-translational
415 activation of PEP carboxylase activity and the conversion of PEP to organic acids
416 (Figueroa et al., 2016), which could be an explanation of our observation of
417 higher T6P and organic acids and lower PEP.

418

419 **Phytochrome depletion alters the rate of label incorporation into metabolites**
420 Increased metabolite pool sizes can be indicative of either increased synthesis or
421 reduced utilisation. To distinguish between these possibilities, we combined time-
422 resolved GC-MS with $^{13}CO_2$ labelling. This allowed us to track both diurnal
423 abundance and flux of newly fixed C to individual metabolites. We again used 35-day
424 old *phyABD* and 35- and 30-day WT as controls and, in a second experiment, younger
425 adult (17-19 d) WT, *phyABD* and *phyABDE* plants. $^{13}CO_2$ labelling was performed
426 from *Zeitgeber* time (ZT) 0 until ZT2 or ZT12, and metabolites were quantified at
427 ZT0, ZT2, ZT12 and ZT24 (Fig. 2A, B). The second experiment was replicated
428 (Supplementary Fig. S2, 'experiment 3'). Our choice of time intervals for labelling
429 was guided by expected label saturation times for different groups of the metabolites
430 detectable by our protocol (Szecowka *et al*, 2013). The heat map (Fig. 2C,
431 Supplementary Fig. S2) shows metabolite abundance and ^{13}C incorporation (^{13}C

432　　enrichment multiplied by pool size, see Methods) as the fold-change ratio between a

433　　given *phy* mutant and WT. Except for some minor differences, the results are broadly

434　　similar in young and more mature adult plants (Fig. 2C, Supplementary Fig. S2-5).

435

436　　The amino acids proline, glutamine and serine over-accumulate in *phy* mutants and

437　　also showed increased ^{13}C incorporation in at least two of the three experiments,

438　　implying faster synthesis from newly fixed carbon (Fig. 2C, Supplementary Fig. S2).

439　　Proline and glutamine are synthesized from 2-oxoglutarate (2-OG), indicating a

440　　potential common up-regulation of biosynthetic processes using 2-OG (Fig. 2E). 2-

441　　OG is less amenable to GC-MS detection, however, our LC-MS/MS data (Fig. 1A,

442　　Supplementary Fig. S1) show that 2-OG levels are not significantly altered by

443　　phyABD deficiency. As other TCA-cycle components are more abundant in *phyABD*,

444　　the increased labelling of proline and glutamine is consistent with increased use of 2-

445　　OG. Phytochrome depletion also increased the levels and rates of synthesis of

446　　raffinose and its precursor *myo*-inositol (Fig. 2C-D), beta-alanine, and in most

447　　experiments, phenylalanine.

448

449　　Several other metabolites that are mildly elevated by phy-depletion, on the whole, did

450　　not exhibit significantly faster ^{13}C labelling, i.e. are not synthesized faster from newly

451　　fixed carbon. Examples include amino acids in the oxaloacetate and pyruvate amino

452　　acid biosynthesis pathways like lysine and threonine, as well as succinate, fumarate

453　　and malate (Fig.2C-E). A similar scenario is observed for glucose and fructose, which

454　　are markedly elevated in *phy* mutants compared to WT but do not show faster

455　　incorporation of newly fixed C, at least at the beginning of the day (Fig. 2C, D,

456　　Supplementary Fig. S2-5). In the WT, the net synthesis of glucose and fructose is

457　　rapid, reaching high levels by ZT2. In comparison, severe *phy* mutants have higher

458　　dawn glucose and fructose content and lower initial rates of labelling, and their

459　　content later rises to reach ~two-fold higher levels at dusk than WT plants. These

460　　differences suggest that both synthesis and utilisation of glucose and fructose are

461　　different in *phy* mutants compared to WT.

462

463　　In summary, our ^{13}C labelling data indicate that in adult plants phy depletion alters the

464　　flux balance to different sets of metabolites with increased synthesis of proline, serine

14

465 and glutamine, a boost of phenylalanine, raffinose and *myo*-inositol synthesis and
466 abundance, and over-accumulation of malate, glucose and fructose.

467

468 **The metabolic response is robust and may be PIF regulated**

469 The phy-dependent SAR is observed in a wide range of conditions. We investigated if
470 the phy-dependent metabolic response of adult plants is equally robust. We quantified
471 the impact of phy depletion on three metabolites - glucose, malate and proline - over a
472 range of growth regimes, including varied photoperiods (8L:16D, 12L:12D and
473 16L:8D), irradiance levels (54, 110 or 190 μmol m^{-2} s^{-1}) or temperatures (16°C or
474 22°C) in 12L:12D (Supplementary Fig. S6A-I). Different photoperiods were applied
475 after two initial weeks in 8L:16D. Light and temperature changes were applied only
476 for the last 3 or 4 days of the experiment, respectively, after growth in standard
477 conditions (18°C, 115μmol m^{-2} s^{-1}) to ensure that plants were of a similar size and
478 developmental stage.

479

480 In all conditions, we observed higher levels of glucose, malate and proline in *phy*
481 multi-allele mutants compared to WT, the only exception being *phyBD* in 8L:16D
482 which had similar glucose levels to WT (Supplementary Fig. S6 A-I). Elevated levels
483 of glucose, malate and proline were observed in *phyABD* mutant lines in the Ler and
484 the Col-0 backgrounds, indicating that higher metabolite levels in *phy* mutants are not
485 accession-specific (Supplementary Fig. S6 J-L). We also established that despite the
486 distinctive *phy* mutant leaf morphology (elongated petioles and smaller blades), the
487 metabolite response was comparable across rosette, leaf blade and petiole tissue
488 (Supplementary Fig. S6M-O). Thus, the impact of phytochrome depletion on glucose,
489 malate and proline levels in adult plants is extremely robust to environmental
490 perturbation and is present across different vegetative tissues. Our observations are
491 broadly similar to those reported for *phyA;phyB;phyC* triple rice mutant leaves at two
492 developmental stages, suggesting conservation of the response across species (Jumtee
493 *et al*, 2009).

494

495 Since the day time abundance and activity of PIF4 and PIF5 is expected to rise in
496 phy-deficient plants we investigated metabolites in p35S:PIF4-HA and p35S:PIF5-
497 HA (Lorrain *et al*, 2008). Both lines showed increased glucose, malate and proline
498 levels. This was not the case for the *hy5* mutant, a positive phy signalling component

15

499 (Supplementary Fig. S6 P-R), indicating that HY5 may not have a prominent role in

500 the phy-metabolite response. However, we cannot rule out a redundant role of HY5

501 with HYH, the HY5 homolog (Holm *et al*, 2002).

502

Phytochrome deactivation alters the expression of metabolic stress signalling

504 Two of the metabolites with increased ^{13}C incorporation, proline and raffinose, are

505 hallmarks of abiotic stress-induced metabolic rearrangements (Krasensky & Jonak,

506 2012). We reasoned that phy deficiency may lead to activation of stress signalling.

507 Therefore, we tested the expression of stress-induced genes that have been implicated

508 in stress-induced metabolic changes: the cold stress coordinator *C-REPEAT*

509 *BINDING FACTOR* (*CBF*)3, *DELTA1-PYRROLINE-5-CARBOXYLATE SYNTHASE*

510 (*P5CS) 2* in the proline biosynthesis pathway and *GALACTINOL SYNTHASE* (*GOLS*)

511 *3* in the raffinose biosynthetic pathway (Gilmour *et al*, 2000; Taji *et al*, 2002; Cook *et*

512 *al*, 2004; Maruyama *et al*, 2009). Expression of all three genes was significantly up-

513 regulated in the daytime in *phyABDE* compared to WT (Supplementary Fig. S7A-C),

514 providing one possible explanation for increased flux in the corresponding

515 biosynthetic pathways. We also established that expression of the cold stress-induced

516 vacuolar glucose transporter *ERDL6* (Poschet *et al*, 2011; Klemens *et al*, 2014) is

517 strongly affected by phy. *ERDL6* transcript levels were much reduced in *phyABDE*

518 and by phy deactivation by an EoD FR pulse (EoD-FR) (Supplementary Fig. S7D-E).

519 As the *erdl6* mutant has high vacuolar glucose and increased freezing tolerance, this

520 opens the possibility that phy controls sugar partitioning and osmotic protection

521 through *ERDL6* regulation (Poschet *et al*, 2011).

522

Quantification of rates of protein synthesis and cell wall synthesis using $^{13}CO_2$
labelling

525 One of the most striking features of severely phy-depleted adult plants is their reduced

526 biomass, which in the case of *phyABDE* is only about 20% of WT plants (Yang *et al*,

527 2016). A probable cause of the substantial biomass disparity is a difference in growth

528 rate. We, therefore, analysed the rates of protein and cell wall synthesis. These are

529 responsible for the vast majority of the metabolic resources deposited as biomass.

530

531 Analysis of fluxes to cellular components can be complicated by incomplete

532 enrichment in precursor pools, for example, enrichment rises slowly and incompletely

533   in many free amino acids (Ishihara et al., (2015). This can result in underestimation of

534   the rate of protein synthesis, and the extent of the underestimation will vary if

535   enrichment in free amino acids differs between conditions or genotypes. To avoid

536   such errors, we employed a method established by Ishihara et al., (2015). Protein

537   synthesis is quantified using data for Ala, for which enrichment rises rapidly to a high

538   level in the free pool. Enrichment in protein-bound Ala is divided by enrichment in

539   free Ala to estimate the absolute rate of protein synthesis (Ks, protein synthesised as a

540   % of existing protein per h). $^{13}CO_2$ was supplied for 24 h, starting before dawn,

541   samples harvested at ZT0, ZT2, ZT12 and ZT24, and analysed by GC-MS to

542   determine enrichment in free Ala and protein-bound Ala. Rates were calculated for

543   the daytime (ZT0-ZT12) and the night (ZT12-ZT24).

544

545   Protein levels were similar in WT and *phyABD*, though slightly lower at the start of

546   the day in younger (17-19 day old) plants (Fig. 3A, Supplementary Fig. S8A). The

547   rates of protein synthesis were very comparable in WT and mutant plants, both in the

548   daytime and at night (Fig. 3B,Supplementary Fig. S8B). The rates of ^{13}C

549   incorporation into glucose in cell wall polysaccharides were investigated in the same

550   samples. This provides information about the rate of synthesis of cellulose and the

551   glucan backbone of hemicellulose. Compared to WT, there was no consistent change

552   in *phyABDE* or *phyABD* (Fig. 3C, Supplementary Fig. S8C). On the assumption that

553   cell wall polymers, and especially cellulose, are not rapidly turned over, glucose

554   incorporation in the cell wall provides a measure of RGR . The data, therefore,

555   suggest that RGR of adult *phy* mutants is similar to that of adult WT plants.

556

557   We considered whether protein degradation might be much faster in the *phy* mutants

558   than in WT plants. Assuming that the glucose in cell wall polymers is not rapidly

559   turned over, the rate of protein degradation, Kd, can then be estimated as the

560   difference between the rates of protein synthesis and of glucose incorporation into the

561   cell wall (Ishihara *et al*, 2015, 2017). Compared to WT, there was no consistent

562   change in the rate of protein degradation in *phyABDE* or *phyABD* (Fig. 3B,

563   Supplementary Fig S8B)

564

565   **Carbon uptake and growth is compromised in *phy* mutant seedlings**

566　As the growth rates of adult *phyABD* and *phyABDE* plants were similar to those of
567　WT plants, we reasoned that their compromised adult biomass might result from
568　reduced growth at an earlier stage in their life history. We found that *phyABD* and
569　*phyABDE* have a reduced rate of net carbon uptake per unit aboveground biomass at
570　two weeks, but not at four weeks after sowing (Fig. 4A, C). Further, sequential
571　harvesting to determine above-ground biomass at 5 or more time points between 9 to
572　35 DAS revealed that RGR was much lower in *phyABD* and *phyABDE* than WT for
573　the first 2 to 2.5 weeks, but subsequently increased to resemble that of WT plants
574　(Fig. 4E).

575

576　In addition to the seedling specific difference in RGR we also found that water
577　content is higher in *phy* mutants at the seedling stage but becomes equivalent to that
578　of the WT at about the same time as RGR (Supplementary Fig. S9A). Since
579　metabolism and growth are often tightly connected, we also measured selected
580　metabolites in 10- and 14-day old seedlings at the end of the day and normalised the
581　values by dry weight (Supplementary Fig. S9B-F). Compared to WT, *phyABD* and
582　*phyABDE* mutants contained higher glucose, as in the adult plants, but lower or
583　similar levels of malate and proline (Supplementary Fig. S9C-E). Notably, the
584　mutants accumulated only a third to half of the amount of starch of the WT, which is
585　fully consistent with the observed reduced carbon uptake (Supplementary Fig. S9F).

586

587　In summary, we find that *phy* mutants grow at a slower rate only at the seedling to
588　young rosette stages, where they also have a lower carbon assimilation rate and a
589　higher water content. Furthermore, metabolic differences between *phy* mutants and
590　WT plants are markedly different at the seedling and adult stages.

591

592　**Phytochrome deficiency at the seedling stage constrains biomass production**
593　It is well known that SAR, caused by phytochrome depletion, leads to large changes
594　in plant architecture including the extension of hypocotyls and petioles and a
595　concomitant reduction in cotyledon and first leaf area (de Wit *et al*, 2015). To account
596　for this, we normalised the rate of seedling photosynthesis on the area of their
597　cotyledons plus first leaves. The rate of photosynthesis per unit area was identical in
598　the *phy* mutant and WT seedlings (Fig. 4B, D). When fluence rates are limiting for
599　photosynthesis, as was the case in our experiments, the rate of whole plant

18

600   photosynthesis depends on how much light the plant intercepts. The smaller cotyledon
601   area per seedling in *phy* mutants will mean that less light is intercepted and there is
602   less photosynthesis per plant. This may limit carbon gain and growth at the seedling
603   stage. The reduced cotyledon area arises from prioritisation of hypocotyl elongation at
604   the expense of cotyledon expansion during early development (de Wit *et al*, 2018).
605   While perhaps counterintuitive, our data also imply that during post-seedling
606   development, the quite dramatic changes in architecture and metabolism (see above)
607   caused by phytochrome inactivation do not impact on rosette biomass gain. Our data
608   also imply that phytochrome action during the seedling stage alone determines final
609   biomass.

610

611   To move beyond correlative observations we used the *Arabidopsis* framework model
612   to test more rigorously whether phytochrome inaction at the seedling stage can cause
613   the extreme adult plant biomass deficit. The framework model was ideal for this
614   purpose as it incorporates molecular mechanisms such as the circadian clock and
615   photosynthesis but also carbon resources partitioning, organ formation and
616   architecture, and can be used to simulate plant growth and development in different
617   environmental conditions (Chew *et al*, 2014). The model was calibrated for the WT to
618   match 27 DAS (days after sowing) biomass data by changing the input light intensity.
619   In our experimental conditions, photosynthesis rather than seed reserves drives
620   growth from day 7 on. Thus to obtain starting parameter values we quantified day 7
621   cotyledon area for WT, *phyABD* and *phyABDE*. We established that by adjusting the
622   day 7 cotyledon area parameter alone, model simulations closely match WT and *phy*
623   mutant cotyledon/leaf area expansion rates during early development (Supplementary
624   Fig. S10). The model also provides a good qualitative match to our measured RGR
625   data, in particular, the model predicts that *phy* mutants grow more slowly than WT
626   plants until about 2 to 2.5 weeks (Fig. 4E, F). Finally, the model can predict with a
627   high degree of accuracy the adult plant biomass (Fig. 4G). Thus, the modelling
628   indicates that small cotyledon area, a hallmark of phytochrome deficient seedlings, is
629   sufficient to severely constrain subsequent biomass accumulation in adult plants.

630

631   **Experimental validation of model prediction**
632   We sought to test more rigorously the model predictions through a lab-based
633   approach that explicitly examined the relationship between the timing of phytochrome

19

634   action, cotyledon development and adult plant biomass. One set of seedlings was
635   grown in 12L:12D low fluence rate light (3μmol m^{-2} s^{-1}) until 9 DAS and then
636   transferred to control conditions (12L:12D 115umol m^{-2} s^{-1}). Low light reduces the
637   activity of phytochromes and other photoreceptors with analogous roles in seedling
638   deetiolation.   Other sets were grown in 12L:12D +/- EoD-FR (which mainly
639   inactivates phyB) until either day 14 or 20, or were grown in 12L:12D +/- EoD-FR
640   between day 15 and 28. As anticipated, low light and EOD-FR treatments from day 1
641   suppressed seedling cotyledon expansion compared to controls, with low fluence rate
642   having the strongest effect (Supplementary Fig. S11A). Importantly, we observed a
643   strong correlation between reduced cotyledon size and subsequent adult plant
644   biomass, with low light provided at the seedling stage leading to a 64% reduction in
645   vegetative biomass (Fig. 4H, Supplementary Fig. S11A, B). Our data also show that
646   EoD-FR applied after 14 days does not affect biomass, despite eliciting the classic
647   SAR phenotype in the later (15-28d) treatment (Fig. 4H).
648
649   Our data experimentally validates the Framework model prediction that slower
650   growth specifically at the seedling stage is sufficient for the reduced biomass of adult
651   multi-allele *phy* mutants.
652
653   **<u>Discussion</u>**
654
655   **Phytochrome controls daytime levels of T6P**
656
657   The starting point for this study was the finding that higher-order *phy* mutants have
658   massively decreased biomass, and elevated levels of several central metabolites
659   including sugars and starch (Yang *et al*, 2016). These observations led us to propose
660   that phytochrome signalling is required for carbon flux and adult plant growth.
661
662   As a first step in this study, we employed LC-MS/MS to analyse phosphorylated and
663   short-lived intermediates (Arrivault *et al*, 2009; Szecowka *et al*, 2013) and to search
664   for the steps in central metabolism under phytochrome control. This method
665   established that levels of metabolites in the lower part of glycolysis (PEP and 3PGA)
666   were decreased and many organics acids were increased in *phy* mutants compared to
667   WT plants. Further, daytime levels of Gal-1-P, Glc-1-P, UDPGlc and especially T6P

20

668   were elevated in *phyABD* (Fig, 1, Supplementary Fig. S1). T6P typically parallels

669   levels of sugars, especially sucrose (Lunn *et al*, 2006; Yadav *et al*, 2014) and

670   therefore its increased abundance in *phy* mutants may be a consequence of sugar over-

671   accumulation (see Fig 2, Supplementary Fig. S2, (Yang *et al*, 2016)). It has been

672   shown using inducible genetics that T6P stimulates flux to organic acids and amino

673   acids and that this involves post-translational activation of PEP carboxylase and

674   nitrate reductase (Figueroa *et al*, 2016). The increase in T6P could explain the

675   increased flux to organics acids and the accompanying decline in the level of PEP and

676   3PGA. It could also have wider consequences. T6P was recently shown to be an

677   indirect modulator of PIF4 activity at higher temperatures (Hwang *et al*, 2019).

678   KIN10, a catalytic subunit of the energy-sensing protein kinase SNF1-RELATED

679   KINASE1 (SnRK1) complex was shown to phosphorylate and destabilize PIF4,

680   preventing its accumulation at high temperatures. Genetic data suggest that T6P can

681   indirectly promote PIF4 action by suppressing the kinase activity of KIN10 (Hwang

682   *et al*, 2019). PIF4 levels and activity are likely to be elevated in phy-deficient plants,

683   and high daytime levels of T6P could potentially augment PIF4 action (Lorrain *et al*,

684   2008; Johansson *et al*, 2014).

685

Phytochrome suppresses stress metabolite synthesis

686

687   Higher levels of sugars, amino acids and organic acids in *phy* mutants could be due to

688   increased production or decreased downstream usage. We used $^{13}CO_2$ labelling

689   coupled with GC-MS to investigate fluxes in central metabolism. This revealed that

690   raffinose, *myo*-inositol, proline, and according to 2 out of 3 of our experiments also

691   serine, glutamine and phenylalanine are synthesized at higher rates in higher-order

692   *phy* mutants (Fig. 2C-E; Supplementary Fig. S2-5).

693

694   In leaves exposed to light, serine is an intermediate of the photorespiration pathway,

695   being formed by glycine decarboxylation in mitochondria. The increased level and

696   labelling of serine in the light in higher-order *phy* mutants was accompanied by no

697   change or even a trend to a decline of glycine and glycerate. Because of these

698   observations we speculate that there may be phytochrome-dependent changes which

699   stimulate glycine decarboxylase activity and/or restrict the conversion of serine to

700   glycerate.

701

702 Phenylalanine is synthesised by the shikimate pathway. Our GC-MS analyses
703 revealed somewhat (but not significantly) higher levels of shikimate in 5-week old
704 higher-order *phy* mutants. Together with the labelling data and a higher levels of
705 phenylalanine in 5-week old plants, these observations point to negative regulation of
706 the shikimate pathway by phytochrome. Phenylalanine is the starting point for the
707 synthesis of a wide range of specialised and stress metabolites.

708

709 Our ^{13}C labelling data suggest that phytochrome negatively affects the biosynthesis of
710 the stress metabolites raffinose, glutamine and proline (Fig. 2C-E). This notion was
711 supported by the increase in transcript abundance for key pathway enzymes, *GOLS3*
712 (raffinose) and *P5CS2* (proline) in *phyABDE*, and their (likely) regulator *CBF3*
713 (Supplementary Fig. S7). The increased flux to glutamine and proline suggests that
714 phytochrome suppresses the synthesis of 2-OG-derived amino acids pathways.
715 Interestingly, in contrast to most other TCA cycle intermediates, 2-OG levels are not
716 increased in *phy* mutants (Fig. 1A), indicating that 2-OG may be increasingly used for
717 the synthesis of these amino acids. The proline and glutamine biosynthesis branch is
718 connected to carbohydrate metabolism via short pathways and their regulation is less
719 energetically costly than other amino acids where synthesis and degradation require
720 multiple reaction steps (Hildebrandt, 2018).

721

722 Proline and raffinose accumulation typically occurs in abiotic stress conditions, such
723 as cold stress, high salinity and drought (Kaplan *et al*, 2004; Kempa *et al*, 2008;
724 Urano *et al*, 2009; Pagter *et al*, 2017). Synthesis of glutamine from glutamate is
725 important for nitrogen assimilation into organic molecules and high nitrogen
726 assimilation rates are predicted to occur during cold stress (Hildebrandt, 2018). Thus,
727 phy depletion appears to elicit features of an abiotic stress response. Concurring with
728 this notion, an earlier study showed that low R:FR treatment shade or *phy* mutations
729 significantly improve freezing tolerance and enhances expression of *CBF3* (Franklin
730 & Whitelam, 2007). We confirm that that *CBF3* has markedly elevated expression in
731 *phyABDE* compared to WT (Supplementary Fig. S7). As *CBF3* overexpression
732 induces metabolic changes with strong similarities to phy deficiency, especially high
733 proline accumulation, this suggests a potential molecular regulatory route for phy
734 (Gilmour *et al*, 2000). As already mentioned, *phyABDE* mutants also exhibited
735 elevated daytime expression of *P5CS2* and *GOLS3*, which code for proline, and

736 raffinose biosynthetic enzymes, respectively (Supplementary Fig. S8) and are known

737 to be involved in the abiotic stress response (Gilmour *et al*, 2000; Taji *et al*, 2002;

738 Fowler & Thomashow, 2002; Gilmour *et al*, 2004; Maruyama *et al*, 2004).

739

740 **Phytochrome controls hexose pool sizes**

741 We established that glucose and fructose rose to significantly higher levels during the

742 daytime in *phy* mutants, even though their synthesis rates from newly fixed C were

743 slower than in WT plants, at least at the beginning of the day (Fig. 2, Supplementary

744 Fig. S2-S5). One possible explanation for hexose over-accumulation would be

745 reduced demand from key consumption processes such as protein synthesis or growth.

746 However, our ^{13}C incorporation analysis showed that flux to protein or cell wall

747 synthesis was similar in phy mutants and WT plants (Fig. 3, Supplementary Fig. S8).

748 An alternative explanation is that elevated sugars could arise from enhanced vacuolar

749 storage. In support of this proposition, we established that phy-deactivation reduces

750 the abundance of transcripts that encode vacuolar transporters including *ERDL6*,

751 which exports glucose to the cytosol (Supplementary Fig. S7). This observation

752 suggests that phy depletion may enhance vacuolar storage and accumulation of

753 sugars. Interestingly the expression of *ERDL6* is suppressed during cold stress

754 (Poschet *et al*, 2011; Klemens *et al*, 2013, 2014). Reduction of this monosaccharide

755 exporter is thought to promote vacuolar accumulation of sugars, aiding plant survival

756 during stress conditions (Klemens *et al*, 2013, 2014). These functional properties of

757 *ERDL6*, are therefore entirely consistent with our findings that phy regulates carbon

758 accumulation and stress physiology.

759 Higher levels of hexoses due to lack of phytochrome have also been observed in

760 species other than Arabidops: rice *phyA phyB phyB* mutants strongly over-accumulate

761 glucose and fructose (Jumtee *et al*, 2009), and tomato *phyB1 phyB2* as well as FR

762 treated tomato plants show an increase in these sugars as well (Courbier *et al*, 2020).

763 Therefore, our observation may have relevance for carbon dynamics in crop species.

764

765 **The metabolic profile of phy mutants differs between developmental stages**

766 **before and after normal RGR is reached**

767 The metabolic phenotype of adult *phy* mutants, with elevated levels of sugars, many

768 organic acids and some amino acids (Supplementary Fig. S6 and (Yang *et al*, 2016))

769 differs from that of seedlings (Supplementary Fig. S9). Temporal tracking in *phyABD*

770 and *phyABDE* at the seedling stage revealed that reference metabolites like malate
771 and proline do not over-accumulate, rather, levels tend to be similar to or lower than
772 WT seedlings. Glucose was slightly increased compared to WT seedlings
773 (Supplementary Fig. S9), in agreement with findings from a recent study (Kozuka *et*
774 *al*, 2020).

775

776 Seedlings and adult plants also differed in how phytochrome deficiency impacted on
777 starch levels. In adult plants, starch remained high or was even slightly elevated in
778 *phy* mutants (Yang *et al*, 2016). In seedlings, starch is decreased by over two-fold
779 (Supplementary Fig. S9). The resulting shift in the balance between starch and
780 glucose, with low starch and high glucose in *phyABD* and *phyABDE* compared to
781 WT, may be functionally important. A recent study with starch biosynthesis mutants
782 *pgm1, pgi1, adg2*, and the starch degradation mutant *sex1* showed that hypocotyl
783 elongation negatively correlates with starch levels (de Wit *et al*, 2018). Mutants with
784 the longest hypocotyls had the lowest starch levels, suggesting that C that is not
785 partitioned to starch is used to support hypocotyl growth. High sugars may contribute
786 to hypocotyl growth by providing a source of C for cell wall synthesis, energy to
787 support ion accumulation and even as a component of the cellular osmotica that drive
788 water uptake and cell expansion. This relationship between starch vs sugar allocation
789 and growth may be particularly clear in very young seedlings, which derive much of
790 their C from seed reserves. Adult plants rely on photosynthesis as a source of C, and
791 starch accumulation and remobilisation are regulated by circadian- and C-signalling
792 to ensure that C is available over the entire 24 h cycle (Graf *et al*, 2010; Stitt &
793 Zeeman, 2012; Mengin *et al*, 2017; Flis *et al*, 2019; Moraes *et al*, 2019). A lesion in
794 diel starch turnover leads to a deficit in C at night, with plants cycling between a C-
795 replete state in the daytime and deleterious C-starvation at night (Usadel *et al*, 2008).
796 It can be anticipated that a shift in the balance of starch and glucose contributes to the
797 extremely elongated hypocotyl phenotype of *phyABD* and *phyABDE* seedlings, but is
798 largely overruled by a combination of circadian and sugar signalling in adult plants.

799

800 We established that in adult phy-deficient plants, glucose, malate and proline over-
801 accumulation is robustly observed over wide-ranging conditions, in petiole as well as
802 blade tissue, and in the Col-0 and Ler accessions (Supplementary Fig. S6). In *phyABD*
803 and *phyABDE*, metabolites begin to over-accumulate after 2 weeks. Importantly, this

804   coincides with the time when mutant relative growth rate (RGR), which is initially

805   slow, has adjusted to WT pace (Fig. 4, Supplementary Fig. S9).

806

807   **Phy action at the seedling stage determines final plant biomass**

808   Multi-allele *phy* mutants at the adult stage exhibit a striking SAR response, with

809   different leaf architecture and markedly reduced biomass compared to WT plants.

810   Despite this, surprisingly, a combination of ^{13}C flux analyses and sequential

811   destructive harvesting revealed that the rates of protein and cell wall synthesis and

812   overall RGR are not compromised in the adult stage *phy* mutants. This

813   counterintuitive result pointed to the seedling stage as having a potentially critical role

814   in determining adult plant biomass. We demonstrated that higher-order *phy* mutant

815   seedlings have reduced net CO_2 uptake on a fresh weight basis, but not on a cotyledon

816   area basis. This identifies smaller cotyledon size as a constraining factor for the rate

817   of photosynthesis per seedling and, hence, the rate of growth of seedlings after they

818   have exited the stage where growth is driven by seed reserves. The slower initial rate

819   of seedling growth resulted in a lower adult plant biomass (Fig. 4A-E). Incidentally,

820   the lower rate of photosynthesis on a seedling basis, combined with the altered sink-

821   source balance due to an increase in the relative size of the hypocotyl compared to the

822   cotyledons, might explain the general trend to lower levels of metabolites and starch

823   in *phy* seedlings, compared to WT plants.

824

825   These ideas were formally tested using the modular Framework model. This model

826   simulates plant growth and development based on environmental conditions of

827   interest and it is possible to alter the initial cotyledon area at the time of seedling

828   establishment (Chew *et al*, 2014). This feature enabled *in silico* testing of the impact

829   of impaired cotyledon expansion on photosynthesis and plant biomass accumulation.

830   Remarkably, by altering starting cotyledon parameters alone, the model was able to

831   simulate cotyledon area expansion, relative growth rate through development, and

832   final plant biomass of WT, *phyABD* and *phyABDE* to a high degree of accuracy (Fig.

833   4G, H, Supplementary Fig. S10). Thus, these Framework model predictions strongly

834   support our proposal that the lower biomass of *phy* mutants at the adult stage can be

835   explained by their smaller cotyledon area at seedling emergence. These ideas were

836   experimentally corroborated by experiments using low fluence rate regimes or phy

837   deactivating EoD-FR treatments. When applied to WT just during seedling

838   development these conditions cause strong correlative reductions in seedling
839   cotyledon size and adult plant biomass. In contrast, daily EoD-FR pulses supplied
840   after the seedling stage led to changes in leaf morphology but had no effect on final
841   biomass (Fig.4H, Supplementary Fig. S11A-B).
842
843   In summary, unexpectedly, despite dramatic changes to leaf architecture and
844   metabolism, phytochrome de-activation does not impair biomass accumulation at the
845   adult stage, at least under our growth conditions. Viewed from the perspective of the
846   life history of the plant, phytochromes play a key role in seedling deetiolation, and
847   this is critical for setting the pace of growth and, ultimately adult plant biomass. In
848   particular, our results and those of others (de Wit *et al*, 2018) highlight the importance
849   of phytochrome signalling for appropriate allocation of resources in early seedling
850   establishment. Whilst a strong SAR response will be important in a low light and
851   shaded niche, it imposes a big biomass penalty in well-lit locations. Phytochrome
852   signalling may play a crucial role in achieving an optimal trade-off between two
853   competing allocation strategies. One is to invest in hypocotyl growth at the expense of
854   cotyledon expansion, in order to gain access to a more favourable light
855   microenvironment. The other is to invest in the development of photosynthetic
856   capacity in order to quickly achieve high rates of photosynthesis per seedling and,
857   hence, the capacity for autonomous growth before seed reserves are depleted.
858   Achieving an optimal balance may be especially important in crowded locations to
859   attain a dominant role in the canopy. Further, in inter-species competition, the optimal
860   trade-off may depend on seed size, with larger seeds allowing a larger relative
861   investment in hypocotyl and petiole extension.
862
863

864   **<u>Supplementary data</u>**
865   Supplementary data are available at JXB online.
866   *Table S1*. Primers for qPCR
867   *Fig. S1*. Metabolite abundance in WT and *phy* mutants measured by LC-MS/MS, as
868   individual plots.
869   *Fig. S2*. Metabolite abundance and label incorporation fold changes in *phy* mutants /
870   WT in labelling experiments 2 and 3 (17 to 19 DAS).

871   *Fig. S3*. Plots showing GC-MS abundance and ^{13}C label incorporation rate ('^{13}C inc.')

872   data of selected metabolites, labelling experiment 1.

873   *Fig. S4*. Plots showing GC-MS abundance and ^{13}C label incorporation rate ('^{13}C inc.')

874   data of selected metabolites, labelling experiment 2.

875   *Fig. S5*. Plots showing GC-MS abundance and ^{13}C label incorporation rate ('^{13}C inc.')

876   data of selected metabolites, labelling experiment 3.

877   *Fig. S6*. Metabolite content in *phy* mutants and WT in different conditions, tissues and

878   genetic backgrounds

879   *Fig. S7*. Expression of abiotic stress signalling genes involved in metabolic responses

880   to stress.

881   *Fig. S8*. Protein turnover and RGR in ^{13}C labelled samples in experiment 1.

882   Fig. S9. Water content in WT and *phy* mutants and metabolites in seedlings

883   normalised by DW.

884   *Fig. S10*. Growth simulation with the Arabidopsis framework model.

885   *Fig. S11*. Relationship between cotyledon size and final fresh weight.

886   *Data S1*. Full GC-MS and LC-MS metabolite data and statistics.

887

888   **Data availability statement**

889   All data supporting the findings of this study are available within the paper and within

890   its supplementary materials published online.

891

892

902

903   **Author contribution**

904 J.K., A.A., V.M., H.I., A.R., J.F., T.M., N.K., M.G.A, R.F., S.A. and T.O. conducted
905 experiments, J.K., A.A., V.M., H.I., A.R., M.S., K.J.H. designed the experiments, J.K.
906 did Matlab simulations, J.K., A.R., T.M., R.F., S.A., T.O., K.J.H. performed data
907 analysis, J.K., A.R.F, M.S. and K.J.H wrote the paper.
908
909

References

Arrivault S, Guenther M, Ivakov A, Feil R, Vosloh D, Van Dongen JT, Sulpice R & Stitt M (2009) Use of reverse-phase liquid chromatography, linked to tandem mass spectrometry, to profile the Calvin cycle and other metabolic intermediates in Arabidopsis rosettes at different carbon dioxide concentrations. *The Plant Journal* **59:** 824–839

Casal JJ (2013) Photoreceptor Signaling Networks in Plant Responses to Shade. *Annual Reviews of Plant Biology* **64:** 403–427

Chen M & Chory J (2011) Phytochrome signaling mechanisms and the control of plant development. *Trends in Cell Biology* **21:** 664–671

Chew YH, Wenden B, Flis A, Mengin V, Taylor J, Davey CL, Tindal C, Thomas H, Ougham HJ, de Reffye P, Stitt M, Williams M, Muetzelfeldt R, Halliday KJ & Millar AJ (2014) Multiscale digital Arabidopsis predicts individual organ and whole-organism growth. *Proceedings of the National Academy of Sciences* **111:** E4127–E4136

Cook D, Fowler S, Fiehn O & Thomashow MF (2004) A prominent role for the CBF cold response pathway in configuring the low-temperature metabolome of Arabidopsis. *Proceedings of the National Academy of Sciences* **101:** 15243–15248

Courbier S, Grevink S, Sluijs E, Bonhomme PO, Kajala K, Van Wees SCM & Pierik R (2020) Far-red light promotes Botrytis cinerea disease development in tomato leaves via jasmonate-dependent modulation of soluble sugars. *Plant, Cell & Environment* **43:** 2769–2781

Cross JM, von Korff M, Altmann T, Bartzetko L, Sulpice R, Gibon Y, Palacios N & Stitt M (2006) Variation of Enzyme Activities and Metabolite Levels in 24 Arabidopsis Accessions Growing in Carbon-Limited Conditions. *Plant Physiology* **142:** 1574–1588

28

Devlin PF, Robson PR, Patel SR, Goosey L, Sharrock RA & Whitelam GC (1999) Phytochrome D acts in the shade-avoidance syndrome in Arabidopsis by controlling elongation growth and flowering time. *Plant Physiology* **119:** 909–915

Figueroa CM, Feil R, Ishihara H, Watanabe M, Kölling K, Krause U, Höhne M, Encke B, Plaxton WC, Zeeman SC, Li Z, Schulze WX, Hoefgen R, Stitt M & Lunn JE (2016) Trehalose 6-phosphate coordinates organic and amino acid metabolism with carbon availability. *Plant Journal* **85:** 410–423

Flis A, Mengin V, Ivakov AA, Mugford ST, Hubberten HM, Encke B, Krohn N, Höhne M, Feil R, Hoefgen R, Lunn JE, Millar AJ, Smith AM, Sulpice R & Stitt M (2019) Multiple circadian clock outputs regulate diel turnover of carbon and nitrogen reserves. *Plant, Cell & Environment* **42:** 549–573

Fowler S & Thomashow MF (2002) Arabidopsis Transcriptome profiling indicates that multiple regulatory pathways are activated during cold acclimation in addition to the CBF cold response pathway. *The Plant Cell* **14:** 1675–1690

Franklin KA, Praekelt U, Stoddart WM, Billingham OE, Halliday KJ & Whitelam GC (2003) Phytochromes B, D, and E act redundantly to control multiple physiological responses in Arabidopsis. *Plant Physiology* **131:** 1340–1346

Franklin KA & Whitelam GC (2005) Phytochromes and shade-avoidance responses in plants. *Annals of Botany* **96:** 169–175

Franklin KA & Whitelam GC (2007) Light-quality regulation of freezing tolerance in Arabidopsis thaliana. *Nature Genetics* **39:** 1410–1413

Gilmour SJ, Fowler SG & Thomashow MF (2004) Arabidopsis transcriptional activators CBF1, CBF2, and CHF3 have matching Functional Activities. *Plant Molecular Biology* **54:** 767–781

Gilmour SJ, Sebolt AM, Salazar MP, Everard JD & Thomashow MF (2000) Overexpression of the Arabidopsis CBF3 transcriptional activator mimics multiple biochemical changes associated with cold acclimation. *Plant Physiology* **124:** 1854–65

Graf A, Schlereth A, Stitt M & Smith AM (2010) Circadian control of carbohydrate availability for growth in Arabidopsis plants at night. *Proceedings of the National Academy of Sciences.* **107:** 9458–9463

Halliday KJ, Salter MG, Thingnaes E & Whitelam GC (2003) Phytochrome control of flowering is temperature sensitive and correlates with expression of the floral

integrator FT. The *Plant Journal* **33:** 875–885

Hildebrandt TM (2018) Synthesis versus degradation: directions of amino acid metabolism during Arabidopsis abiotic stress response. *Plant Molecular Biology* **98:** 121–135

Holm M, Ma LG, Qu LJ & Deng XW (2002) Two interacting bZIP proteins are direct targets of COP1-mediated control of light-dependent gene expression in Arabidopsis. *Genes and Development* **16:** 1247–1259

Hu W, Franklin KA, Sharrock RA, Jones MA, Harmer SL & Lagarias JC (2013) Unanticipated regulatory roles for Arabidopsis phytochromes revealed by null mutant analysis. *Proceedings of the National Academy of Sciences* **110:** 1542–1547

Huege J, Götze JP, Dethloff F, Junker B & Kopka J (2014) Quantification of Stable Isotope Label in Metabolites via Mass Spectrometry. *Methods in Molecular Biology* **1056:** 213–223

Hwang G, Kim S, Cho J, Paik I, Kim J & Oh E (2019) Trehalose□6□phosphate signaling regulates thermoresponsive hypocotyl growth in Arabidopsis thaliana. *EMBO Reports***:** e47828

Ishihara H, Moraes TA, Pyl ET, Schulze WX, Obata T, Scheffel A, Fernie AR, Sulpice R & Stitt M (2017) Growth rate correlates negatively with protein turnover in Arabidopsis accessions. The *Plant Journal* **91:** 416–429

Ishihara H, Obata T, Sulpice R, Fernie AR & Stitt M (2015) Quantifying Protein Synthesis and Degradation in Arabidopsis by Dynamic $^{13}CO_2$ Labeling and Analysis of Enrichment in Individual Amino Acids in Their Free Pools and in Protein. Plant Physiology **168**: 74-93

Johansson H, Jones HJ, Foreman J, Hemsted JR, Stewart K, Grima R & Halliday KJ (2014) Arabidopsis cell expansion is controlled by a photothermal switch. *Nature Communications* **5:** 4848

Jumtee K, Okazawa A, Harada K, Fukusaki E, Takano M & Kobayashi A (2009) Comprehensive metabolite profiling of phyA phyB phyC triple mutants to reveal their associated metabolic phenotype in rice leaves. *Journal of Biosciience and Bioengineering* **108:** 151–159

Kaplan F, Kopka J, Haskell DW, Zhao W, Schiller KC, Gatzke N, Sung DY, Guy CL, Molecular P, Program CB & K EHF (2004) Exploring the Temperature-Stress Metabolome. *Plant Physiology* **136:** 4159–4168

Kempa S, Krasensky J, Santo SD, Kopka J & Jonak C (2008) A Central Role of Abscisic Acid in Stress-Regulated Carbohydrate Metabolism. *PLoS One* **3:** e3935

Kim D, Pertea G, Trapnell C, Pimentel H, Kelley R & Salzberg SL (2013) TopHat2: accurate alignment of transcriptomes in the presence of insertions, deletions and gene fusions. *Genome Biology* **14:** R36

Kircher S & Schopfer P (2012) Photosynthetic sucrose acts as cotyledon-derived long-distance signal to control root growth during early seedling development in Arabidopsis. *Proceedings of the National Academy of Sciences* **109:** 11217–11221

Klemens PAW, Patzke K, Deitmer J, Spinner L, Le Hir R, Bellini C, Bedu M, Chardon F, Krapp A & Neuhaus HE (2013) Overexpression of the Vacuolar Sugar Carrier AtSWEET16 Modifies Germination, Growth, and Stress Tolerance in Arabidopsis. *Plant Physiology* **163:** 1338–1352

Klemens PAW, Patzke K, Trentmann O, Poschet G, Michael B, Schulz A, Marten I, Hedrich R & Neuhaus HE (2014) Overexpression of a proton-coupled vacuolar glucose exporter impairs freezing tolerance and seed germination. *New Phytologist* **202:** 188–197

Kölling K, George GM, Künzli R, Flütsch P & Zeeman SC (2015) A whole ⬜ plant chamber system for parallel gas exchange measurements of Arabidopsis and other herbaceous species. *Plant Methods* **11:48**

Kozuka T, Sawada Y, Imai H, Kanai M, Hirai MY, Mano S, Uemura M, Nishimura M, Kusaba M & Nagatani A (2020) Regulation of sugar and storage oil metabolism by phytochrome during de-etiolation. *Plant Physiology* **182:** 1114–1129

Krasensky J & Jonak C (2012) Drought , salt , and temperature stress-induced metabolic rearrangements and regulatory networks. *Journal of Experimental Botany* **63:** 1593–1608

Legris M, Ince YC & Fankhauser C (2019) Molecular mechanisms underlying phytochrome- controlled morphogenesis in plants. *Nature Communications* **10:5219**

Leivar P, Monte E, Oka Y, Liu T, Carle C, Castillon A, Huq E & Quail PH (2008) Multiple Phytochrome-Interacting bHLH Transcription Factors Repress Premature Seedling Photomorphogenesis in Darkness. *Current Biology* **18:**

1815–1823

Leivar P, Tepperman JM, Cohn MM, Monte E, Al-Sady B, Erickson E & Quail PH
(2012) Dynamic Antagonism between Phytochromes and PIF Family Basic
Helix-Loop-Helix Factors Induces Selective Reciprocal Responses to Light and
Shade in a Rapidly Responsive Transcriptional Network in Arabidopsis. The
Plant Cell **24:** 1398–1419

Lilley-Steward JL, Gee CW, Sairanen I, Ljung K & Nemhauser JL (2012) An
Endogenous Carbon-Sensing Pathway Triggers Increased Auxin Flux and
Hypocotyl Elongation. *Plant Physiology* **160:** 2261–2270

Lisec J, Schauer N, Kopka J, Willmitzer L & Fernie AR (2006) Gas chromatography
mass spectrometry-based metabolite profiling in plants. *Nature Protocols* **1:**
387–396

Lorrain S, Allen T, Duek PD, Whitelam GC & Fankhauser C (2008) Phytochrome-
mediated inhibition of shade avoidance involves degradation of growth-
promoting bHLH transcription factors. The *Plant Journal* **53:** 312–323

Lun ATL, Chen Y & Smyth GK (2016) It's DE-licious: A Recipe for Differential
Expression Analyses of RNA-seq Experiments Using Quasi-Likelihood Methods
in edgeR. *Statistical Genomics* **1418:** 391–416

Lunn JE, Delorge I, Figueroa CM, Van Dijck P & Stitt M (2014) Trehalose
metabolism in plants. The *Plant Journal* **79:** 544–567

Lunn JE, Feil R, Hendriks JHM, Gibon Y, Morcuende R, Osuna D, Scheible W-R,
Carillo P, Hajirezaei M-R & Stitt M (2006) Sugar-induced increases in trehalose
6-phosphate are correlated with redox activation of ADPglucose
pyrophosphorylase and higher rates of starch synthesis in *Arabidopsis thaliana*.
The *Biochemical Journal* **397:** 139–48

Mancini E, Iserte J, Yanocsky M & Chernomoretz A (2019) ASpli: Analysis of
alternative splicing using RNA-Seq. *1.8.1. ed.* **Bioconduct**

Maruyama K, Sakuma Y, Kasuga M, Ito Y, Seki M, Goda H, Shimada Y, Yoshida S,
Shinozaki K & Yamaguchi-Shinozaki K (2004) Identification of cold-inducible
downstream genes of the Arabidopsis DREB1A/CBF3 transcriptional factor
using two microarray systems. The *Plant Journal* **38:** 982–993

Maruyama K, Takeda M, Kidokoro S, Yamada K, Sakuma Y, Urano K, Fujita M,
Yoshiwara K, Matsukura S, Morishita Y, Sasaki R, Suzuki H, Saito K, Shibata
D, Shinozaki K & Yamaguchi-Shinozaki K (2009) Metabolic Pathways Involved

in Cold Acclimation Identified by Integrated Analysis of Metabolites and Transcripts Regulated by DREB1A and DREB2A. *Plant Physiology* **150:** 1972–1980

Mengin V, Stitt M, Pyl ET & Moraes TA (2017) Photosynthate partitioning to starch in Arabidopsis thaliana is insensitive to light intensity but sensitive to photoperiod due to a restriction on growth in the light in short photoperiods. *Plant, Cell &Environment* **40:** 2608–2627

Moraes TA, Mengin V, Annunziata MG, Encke B, Krohn N, Höhne M & Stitt M (2019) Response of the Circadian Clock and Diel Starch Turnover to One Day of Low Light or Low CO_2. *Plant Physiology* **179:** 1457–1478

Oyama T, Shimura Y & Okada K (1997) The Arabidopsis HY5 gene encodes a bZIP protein that regulates stimulus- induced development of root and hypocotyl. *Genes and Development* **11:** 2983–2995

Pagter M, Alpers J, Erban A, Kopka J, Zuther E & Hincha DK (2017) Rapid transcriptional and metabolic regulation of the deacclimation process in cold acclimated Arabidopsis thaliana. *BMC Genomics* **18:** 731

Poschet G, Hannich B, Raab S, Jungkunz I, Klemens PAW, Krueger S, Wic S, Neuhaus HE & Buttner M (2011) A Novel Arabidopsis Vacuolar Glucose Exporter Is Involved in Cellular Sugar Homeostasis and Affects the Composition of Seed Storage Compounds. *Plant Physiology* **157:** 1664–1676

Rausenberger J, Hussong A, Kircher S, Kirchenbauer D, Timmer J, Nagy F, Schäfer E & Fleck C (2010) An integrative model for phytochrome B mediated photomorphogenesis: From protein dynamics to physiology. *PLoS One* **5:** e10721

Robinson MD, McCarthy DJ & Smyth GK (2009) edgeR: A Bioconductor package for differential expression analysis of digital gene expression data. *Bioinformatics* **26:** 139–140

Sánchez-Lamas M, Lorenzo CD & Cerdán PD (2016) Bottom-up Assembly of the Phytochrome Network. *PLoS Genetics* **12:** e1006413

Stewart JL, Maloof JN & Nemhauser JL (2011) PIF Genes Mediate the Effect of Sucrose on Seedling Growth Dynamics. *PLoS One* **6:** e19894

Stitt M & Zeeman SC (2012) Starch turnover: Pathways, regulation and role in growth. *Current Opinionin Plant Biology* **15:** 282–292

Szecowka M, Heise R, Tohge T, Nunes-Nesi A, Vosloh D, Huege J, Feil R, Lunn J,

Nikoloski Z, Stitt M, Fernie AR & Arrivault S (2013) Metabolic fluxes in an illuminated Arabidopsis rosette. *The Plant Cell* **25:** 694–714

Taji T, Ohsumi C, Iuchi S, Seki M, Kasuga M, Kobayashi M, Yamaguchi-Shinozaki K & Shinozaki K (2002) Important roles of drought- and cold-inducible genes for galactinol synthase in stress tolerance in Arabidopsis thaliana. The *Plant Journal* **29:** 417–426

Urano K, Maruyama K, Ogata Y, Morishita Y, Takeda M & Sakurai N (2009) Characterization of the ABA-regulated global responses to dehydration in Arabidopsis by metabolomics. The *Plant Journal* **57:** 1065–1078

Usadel B, Bläsing OE, Gibon Y, Retzlaff K, Höhne M, Günther M & Stitt M (2008) Global transcript levels respond to small changes of the carbon status during progressive exhaustion of carbohydrates in Arabidopsis rosettes. *Plant Physiology* **146:** 1834–1861

de Wit M, George GM, Ince YÇ, Dankwa-Egli B, Hersch M, Zeeman SC & Fankhauser C (2018) Changes in resource partitioning between and within organs support growth adjustment to neighbor proximity in Brassicaceae seedlings. *Proceedings of the National Academy of Sciences* **115:** E9953–E9961

de Wit M, Ljung K & Fankhauser C (2015) Contrasting growth responses in lamina and petiole during neighbor detection depend on differential auxin responsiveness rather than different auxin levels. *New Phytologist* **208:** 198–209

Woodrow P, Ciarmiello LF, Annunziata MG, Pacifico S, Iannuzzi F, Mirto A, D'Amelia L, Dell'Aversana E, Piccolella S, Fuggi A & Carillo P (2017) Durum wheat seedling responses to simultaneous high light and salinity involve a fine reconfiguration of amino acids and carbohydrate metabolism. *Physiologia Plantarum* **159:** 290–312

Yadav UP, Ivakov A, Feil R, Duan GY, Walther D, Giavalisco P, Piques M, Carillo P, Hubberten HM, Stitt M & Lunn JE (2014) The sucrose-trehalose 6-phosphate (Tre6P) nexus: Specificity and mechanisms of sucrose signalling by. *Journal of Experimental Botany* **65:** 1051–1068

Yang D, Seaton DD, Krahmer J & Halliday KJ (2016) Photoreceptor effects on plant biomass, resource allocation, and metabolic state. *Proceedings of the National Academy of Sciences* **113:** 7667–7672

Zhang R, Calixto CPG, Marquez Y, Venhuizen P, Tzioutziou NA, Guo W, Spensley M, Entizne JC, Lewandowska D, Have S Ten, Frey NF, Hirt H, James AB,

Nimmo HG, Barta A, Kalyna M & Brown JWS (2017) A high quality Arabidopsis transcriptome for accurate transcript-level analysis of alternative splicing. *Nucleic Acids Research* **45:** 5061–5073

Figure legends

Figure 1: Metabolite abundance measured by LC-MS/MS at ZT6 and ZT24 in *phyABD* at 35 DAS, a same-age WT control (35 DAS) and a same biomass WT control (30 DAS). (A) Heatmap representing the fold change in *phyABD* over either of the WT controls. Blue: fold change > 1, red: fold change < 1. * $p<0.05$ in Welch's t-test comparing WT and *phyABD* of the same time point. n=3. (B) Plots of the abundance of metabolites with a significant decrease or increase in *phyABD*, and sucrose-6-phosphate. # $p<0.05$ *phyABD* vs. WT 30 DAS, * $p<0.05$ *phyABD* vs WT 35 DAS. Samples were harvested and frozen inside the incubator to preserve phosphorylated and short-lived metabolites. ADPGlc: ADP-glucose, T6P: trehalose-6-phosphate, Gal1P: galactose-1-phosphate, UDPGlc: UDP-glucose, G1,6BP: glucose-1,6-bisphosphate, Glc1P: glucose-1-phosphate, Gly3P: glycerol-6-phosphate, Fru6P: fructose-6-phosphate, Suc6P: sucrose-6-phosphate, 2-O-G: 2-oxo-glutarate, Glc6P: glucose-6-phosphate, 3-PGA: 3-phospho-glycerate, Man6P: mannose-6-phosphate, FBP: fructose-bisphosphate, PEP: phospho-enol-pyruvate
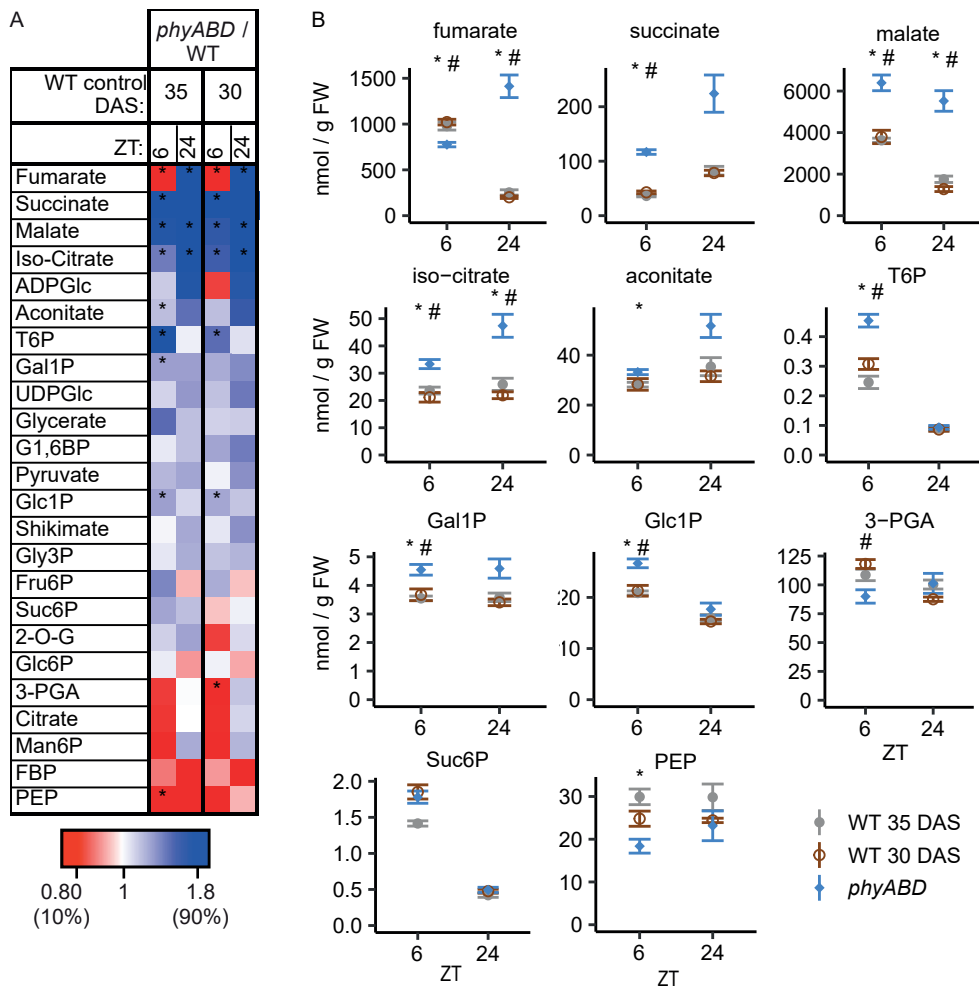
Figure 2: GC-MS analysis of metabolite abundance and ¹³C label incorporation in phy mutants and WT controls. (A) Timing of ¹³C labeling and sampling. (B) Workflow of sample preparation for GC-MS and data analysis. Rate of ¹³C label incorporation for the most suitable time point was calculated by multiplying the abundance at a given time point by the fraction of ¹³C in the metabolite at the same time point. (C) Heatmap displaying fold change in abundance (left) and rate of ¹³C label incorporation (right, '¹³C inc.') of *phy* mutant / WT control in 2 independent experiments. For experiment 1, fold change in *phyABD* is shown compared to the same age and same biomass controls, for experiment 2, fold change over WT is shown for *phyABD* and *phyABDE*. All abundance time points are shown, but for the rate of label incorporation only the most suitable time interval was used (time indicated in the rightmost column), which was determined by the latest time point

before label saturation (typically 2 or 12h). Rows are sorted by decreasing average fold change in label incorporation. Blue and red denote higher and lower values in the phy mutant, respectively. Grey: values that could not be determined. * p < 0.05, two-sided t-test, n=3. (D) Plots of abundance and label incorporation of selected metabolites from experiment 1. (E) Simplified and generalized daytime metabolic pathway map illustrating the observed changes in abundance and ^{13}C incorporation. P: phosphate, GABA: gamma-amino-butyrate, Glc: glucose, 3-PGA: 3-phospho-glycerate, PEP: phospho-enol-pyruvate
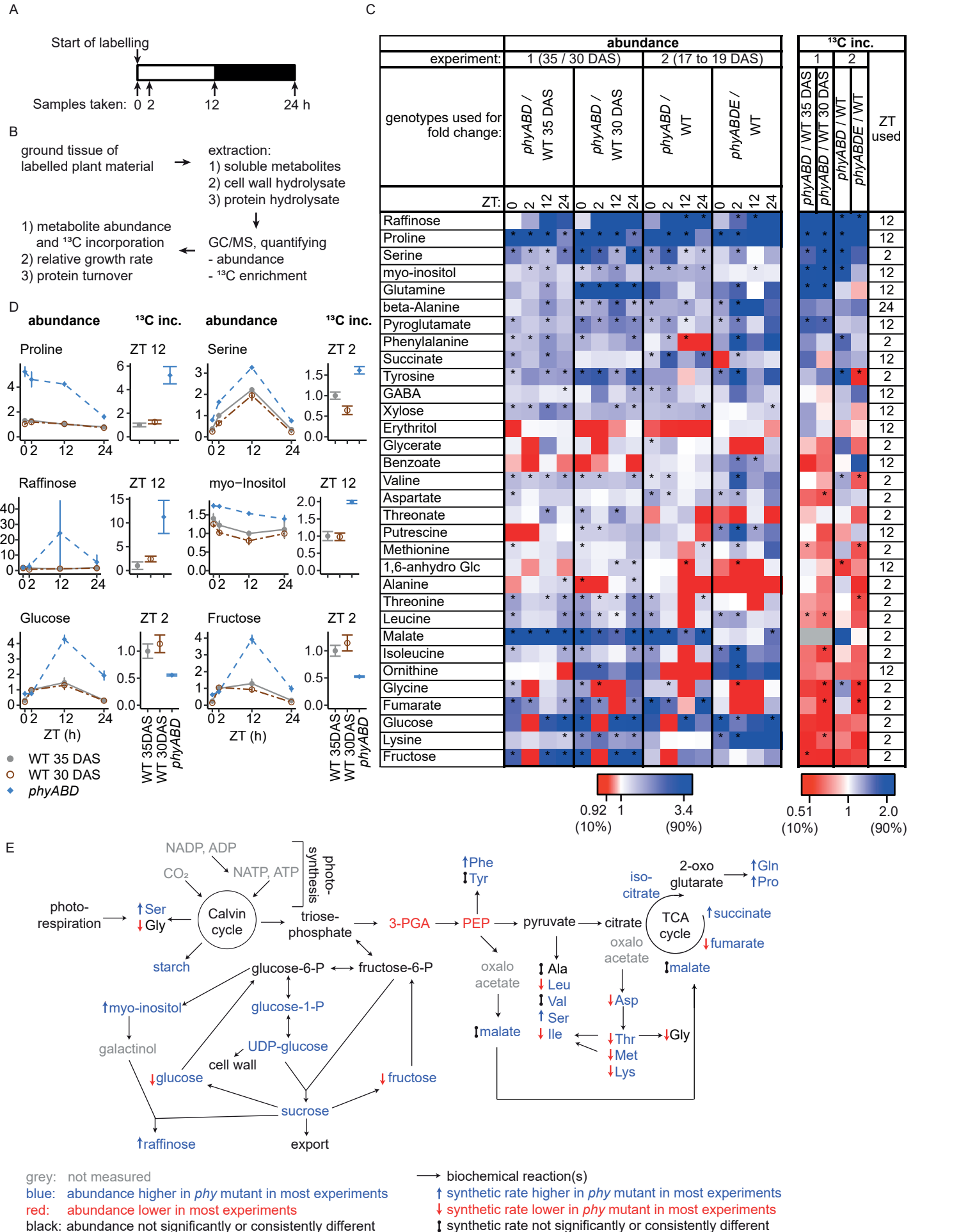
Fig. 3. Protein turnover and relative growth rate (RGR) in ^{13}C labelled samples in experiment 2. (A) Protein content for WT, *phyABD* and *phyABDE* (B) Protein synthetic rate (Ks) was calculated from the incorporation of ^{13}C into alanine in protein, adjusted by ^{13}C incorporation into free alanine. Degradation rates (Kd) were determined by subtracting RGR from Ks (see methods and Ishihara et al. 2015). (C) RGR (= gain in biomass per day / pre-existing biomass) was calculated from ^{13}C incorporation into cell wall cellulose. ^{13}C incorporation at ZT12 was used for calculation of day time RGR, at ZT24 for overall RGR, and the difference between ZT12 and ZT24 for night time RGR. Error bars: (propagated) SEM. * = p < 0.05 (Welch t-test, *phyABDE* mutant vs. WT in panel (A)). No significant differences were found between *phy* mutants and WT in panels B and C (p > 0.05; Welch's t-test). n = 3.

Fig. 4. Final biomass deficit of phy mutants is primarily due to a reduction in RGR early in development, likely because of the reduced cotyledon size in *phy* mutants. (A-D) Net carbon uptake in 2 (A,B) or 4 (C,D) week old plants per unit biomass (A,C) or leaf area (B,D). In A and B, 4 replicates were measured where each replicate consisted of a pot with at least 20 seedlings. 6 replicates, each consisting of one pot with 2 or 3 plants were measured in C and D. (E-G) Cotyledon data at emergence was used to predict RGR and final biomass using the Arabidopsis framework model. E) Destructive RGR time course measurement, n>=10 plants per time point and genotype. (F) Simulated RGR time course of WT, *phyABD* and *phyABDE*. (G) measured and simulated biomass at 27 DAS, n= 36 individual plants per genotype. (H) Biomass at 28 DAS after EoD-FR treatment either at the seedling stage (1-14 DAS) or only after the seedling stage (15-28 DAS) or from 1 to 20 DAS,

or after growth in low light from 1 to 8 DAS ('LL'). 'WL': white light without any EoD-FR or LL treatments. Representative photographs of rosettes at the time of biomass measurement are under the x-axis label. n = 24.*$p < 0.05$ in two-sided Welch's t-test compared to WT (A-G), in the case of (G) WT in data or simulation, and in (H) compared to WL. No significant differences between experimental and simulation data were found in (G).
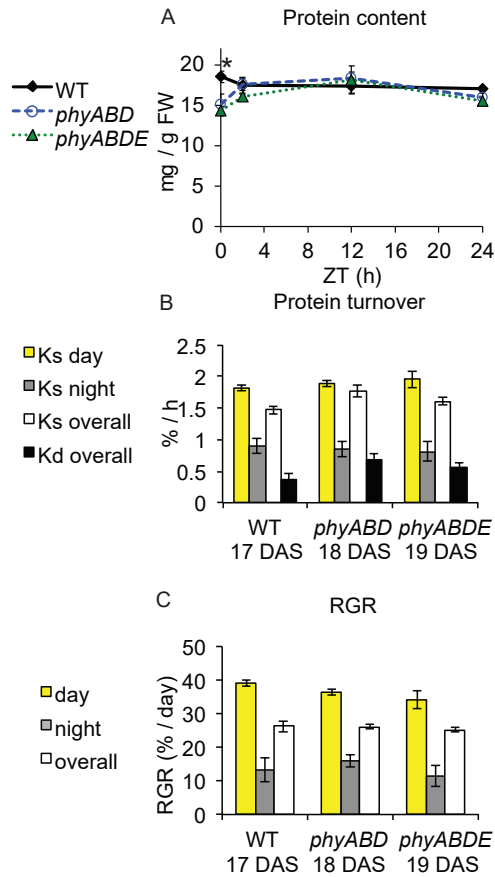
Figure 1: Metabolite abundance measured by LC-MS/MS at ZT6 and ZT24 in *phyABD* at 35 DAS, a same-age WT control (35 DAS) and a same biomass WT control (30 DAS). (A) Heatmap representing the fold change in *phyABD* over either of the WT controls. Blue: fold change > 1, red: fold change < 1. * p<0.05 in Welch's t-test comparing WT and *phyABD* of the same time point. n=3. (B) Plots of the abundance of metabolites with a significant decrease or increase in *phyABD,* and sucrose-6-phosphate. # p<0.05 *phyABD* vs. WT 30 DAS, * p<0.05 *phyABD* vs WT 35 DAS. Samples were harvested and frozen inside the incubator to preserve phosphorylated and short-lived metabolites. ADPGlc: ADP-glucose, T6P: trehalose-6-phosphate, Gal1P: galactose-1-phosphate, UDPGlc: UDP-glucose, G1,6BP: glucose-1,6-bisphosphate, Glc1P: glucose-1-phosphate, Gly3P: glycerol-6-phosphate, Fru6P: fructose-6-phosphate, Suc6P: sucrose-6-phosphate, 2-O-G: 2-oxo-glutarate, Glc6P: glucose-6-phosphate, 3-PGA: 3-phospho-glycerate, Man6P: mannose-6-phosphate, FBP: fructose-bisphosphate, PEP: phospho-enol-pyruvate

Figure 2: GC-MS analysis of metabolite abundance and ¹³C label incorporation in *phy* mutants and WT controls. (A) Timing of ¹³C labeling and sampling. (B) Workflow of sample preparation for GC-MS and data analysis. Rate of ¹³C label incorporation for the most suitable time point was calculated by multiplying the abundance at a given time point by the fraction of ¹³C in the metabolite at the same time point. (C) Heatmap displaying fold change in abundance (left) and rate of ¹³C label incorporation (right, '¹³C inc.') of *phy* mutant / WT control in 2 independent experiments. For experiment 1, fold change in *phyABD* is shown compared to the same age and same biomass controls, for experiment 2, fold change over WT is shown for *phyABD* and *phyABDE*. All abundance time points are shown, but for the rate of label incorporation only the most suitable time interval was used (time indicated in the rightmost column), which was determined by the latest time point before label saturation (typically 2 or 12h). Rows are sorted by decreasing average fold change in label incorporation. Blue and red denote higher and lower values in the *phy* mutant, respectively. Grey: values that could not be determined. * p < 0.05, two-sided t-test, n=3. (D) Plots of abundance and label incorporation of selected metabolites from experiment 1. (E) Simplified and generalized daytime metabolic pathway map illustrating the observed changes in abundance and ¹³C incorporation. P: phosphate, GABA: gamma-amino-butyrate, Glc: glucose, 3-PGA: 3-phospho-glycerate, PEP: phospho-enol-pyruvate

A Protein content

B Protein turnover

C RGR

Figure 3: Protein turnover and relative growth rate (RGR) in ¹³C labelled samples in experiment 2. (A) Protein content for WT, *phyABD* and *phyABDE* (B) Protein synthetic rate (Ks) was calculated from incorporation of ¹³C into alanine in protein, adjusted by ¹³C incorporation into free alanine. Degradation rates (Kd) were determined by subtracting RGR from Ks (see methods and Ishihara et al. 2015). (C) RGR (= gain in biomass per day / pre-existing biomass) was calculated from ¹³C incorporation into cell wall cellulose. ¹³C incorporation at ZT12 was used for calculation of day time RGR, at ZT24 for overall RGR, and the difference between ZT12 and ZT24 for night time RGR. Error bars: (propagated) SEM. * = $p < 0.05$ (Welch's t-test, *phyABDE* mutant vs. WT in panel (A)). No significant differences were found between *phy* mutants and WT in panels B and C ($p > 0.05$; Welch's t-test). n = 3 biological replicates.
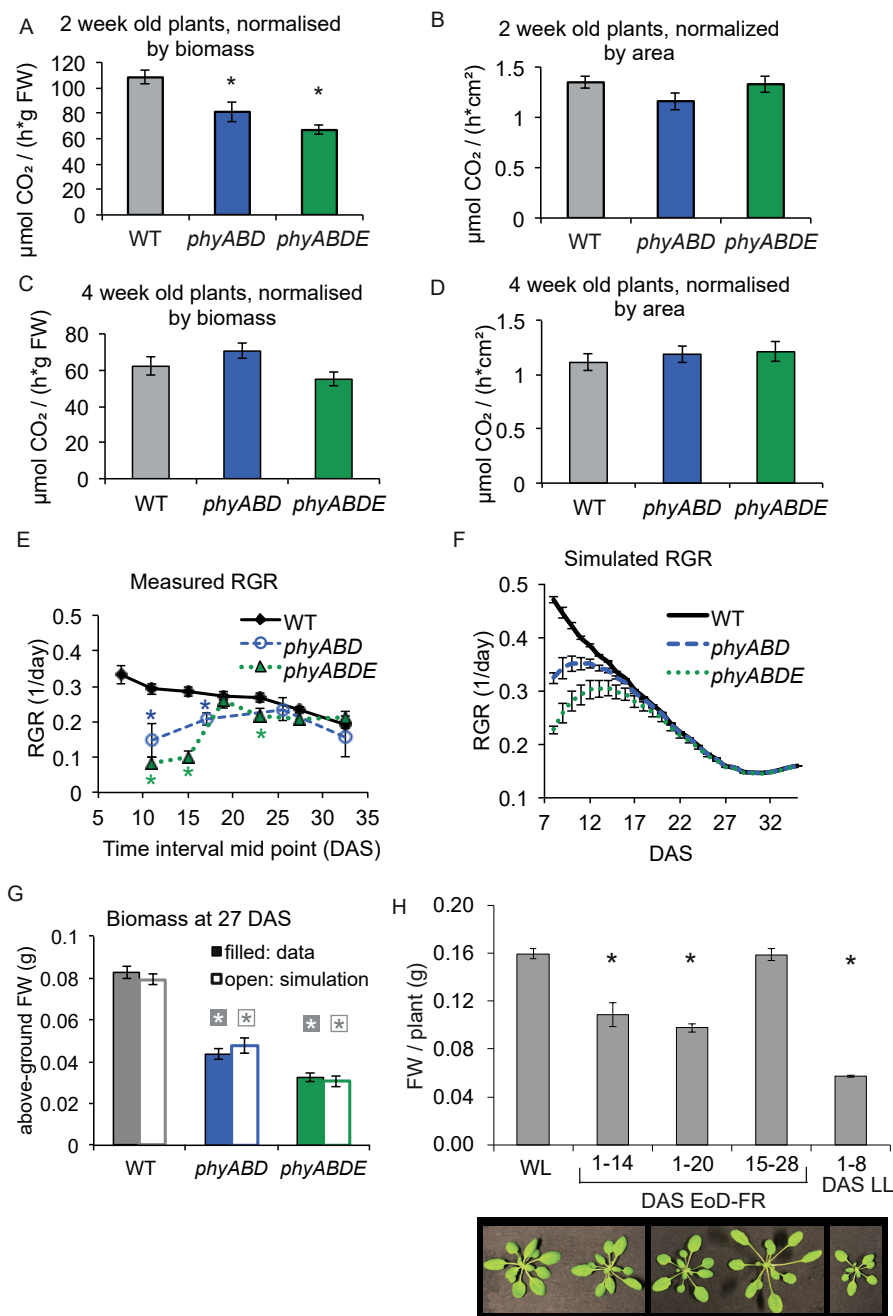
Figure 4: Final biomass deficit of *phy* mutants is primarily due to reduction in RGR early in development, likely because of the reduced cotyledon size in *phy* mutants.

(A-D) Net carbon uptake in 2 (A,B) or 4 (C,D) week old plants per unit biomass (A,C) or leaf area (B,D). In A and B, 4 replicates were measured where each replicate consisted of a pot with at least 20 seedlings. 6 replicates, each consisting of one pot with 2 or 3 plants were measured in C and D. (E-G) Cotyledon data at emergence was used to predict RGR and final biomass using the *Arabidopsis* framework model. E) Destructive RGR time course measurement, n>=10 plants per time point and genotype. (F) Simulated RGR time course of WT, *phyABD* and *phyABDE*. (G) measured and simulated biomass at 27 DAS, n= 36 individual plants per genotype. (H) Biomass at 28 DAS after EoD-FR treatment either at the seedling stage (1-14 DAS) or only after the seedling stage (15-28 DAS) or from 1 to 20 DAS, or after growth in low light from 1 to 8 DAS ('LL'). 'WL': white light without any EoD-FR or LL treatments. Representative photographs of rosettes at the time of biomass measurement are under the x-axis label. n = 24. *$p < 0.05$ in two-sided Welch's t-test compared to WT (A-G), in the case of (G) WT in data or simulation, and in (H) compared to WL. No significant differences between experimental and simulation data were found in (G).